counterpart of this situation cannot be explained in terms of the Fermi surface nesting concept, and the occurrence of a structural modulation in low-dimensional metals does not necessarily originate from a Fermi surface nesting.

On the basis of our finding that analogies exist between the concepts of chemistry and solid-state physics dealing with structural instabilities, one should not neglect one picture over the other. For example, the incommensurate nature of the CDW vectors in the Magnêli phase Mo_4O_{11}, the monophosphate tungsten bronzes, and the blue bronzes $A_{0.33}MoO_3$ (A = K, Rb, or Tl) are easily explained by employing the concept of Fermi surface nesting. On the other hand, why these materials possess 1D-like electronic structures can be easily understood by analyzing the distortion patterns of their MO_6 octahedra.[9b] In general, the concept of Fermi surface nesting allows one to predict the symmetry of the distorted lattice resulting from a CDW instability, but it does not provide a detailed local bonding picture. The opposite is the case with the concepts of local chemical bonding. Thus, the concept of Fermi surface nesting is complementary to that of local chemical bonding.

Acknowledgment. This work was supported by the U.S. Department of Energy, Office of Basic Sciences, Division of Materials Sciences, under Grant DE-FG05-86ER45259, by NATO, Scientific Affairs Division, and by Centre National de la Recherche Scientifique, France.

Solvent Structure around Cations Determined by ^1H ENDOR Spectroscopy and Molecular Dynamics Simulation

M. Sivaraja,[†] T. R Stouch,[‡] and G. C. Dismukes*,[†]

Contribution from the Department of Chemistry, Princeton University, Princeton, New Jersey 08544, and Department of Macromolecular Modelling, Bristol-Myers Squibb, Princeton, New Jersey 08543. *Received July 22, 1991*

Abstract: Classical molecular dynamics simulations of metal ion solvation have been found to confirm the experimental ^1H ENDOR and EPR spectroscopic results on the coordination structure of water molecules surrounding paramagnetic Mn^{2+} ions in frozen aqueous solutions. The well-known simplification and intensification of the six-line Mn^{2+} EPR signal in frozen solutions upon reducing the pH was found to coincide with the appearance of three strong ^1H ENDOR resonances, reflecting symmetrization of the first two solvation shells. From the dipolar part of the hyperfine interaction, the Mn–H distances for the first and second shells were determined to be 2.87 and 4.8 Å, respectively. All protons in the first shell were located at the same distance. Classical molecular dynamics simulations confirmed the experimental distances to both shells using a three-point flexible water model which included electrostatic and van der Waals interactions to Mn^{2+}. At 50 K, the structured second shell of the Mn–H radial distribution function is comprised of 18 water molecules, reflecting disorder which becomes dynamically averaged at 300 K as the second shell expands to encompass on average 22 H_2O molecules at a mean distance of 5.0 Å. The ENDOR and dynamics results support the proposed model of second-shell solvent fluctuation of the Mn^{2+} ligand field splitting as the mechanism for electron spin relaxation of Mn^{2+}. These results should encourage the use of classical molecular dynamics simulations to predict solvation structure of nonparamagnetic ions for which experimental data are not readily available.

This study examines the general question of the solvent structure surrounding metal ions in disordered systems.[1] The absence of long range order makes such systems particularly difficult to study. As a class of matter, disordered systems are extremely common. Specifically, we have choosen Mn^{2+} ions in water because solvation can be measured spectroscopically and modeled theoretically using realistic assumptions. While there are various methods to examine the first-shell solvation structure, the structure of the second shell is difficult to observe by direct methods. An accurate picture of metal ion solvation extending out to the second solvation shell should be obtainable in principle by combining high-resolution electron-nuclear double resonance spectroscopy (ENDOR) and classical molecular dynamics simulations. These tools have not been combined previously to study ion solvation. The ENDOR method enables measurement of the distance between a paramagnetic metal ion and the surrounding solvent nuclei from their ^1H hyperfine interaction.[1,2] Classical molecular dynamics simulations of water solvation, when parametrized with accurate molecular structure and thermodynamic data, can aid in the interpretation of data on intermolecular structure and the dynamics of ion solvation.[3]

Mn^{2+} in aqueous solution exists essentially as the hexaaquo ion at pH below the pK_a (10.5). The stability constants for the complexes with the counterions $[Mn(H_2O)_5X]^+$, Cl^- (0.04 M^{-1}), and ClO_4^- are low, so they are not major species.[4] Evidence for a change in solvation upon freezing is seen in the 10–100-fold reduction in the EPR signal intensity and the broadening of its six-line ^{55}Mn hyperfine structure. This arises from the freezing in of solvent configurations of low symmetry, which removes the 5-fold degeneracy of the spin $S = {}^5/_2$, so called zero-field splitting (ZFS). In fluid solutions, solvent fluctuations tend to average out the static disorder which can be trapped by freezing. The lifetime for water exchange in the first shell in fluid solutions, 2×10^{-7} s, is too slow to dynamically averaged the characteristic ZFS frequencies imposed by low symmetry solvent coordination ($\sim 10^2$–10^4 MHz).[5a] Hence, the first coordination shell must rapidly fluctuate around an equilibrium cubic symmetry. This led to the model postulating that the correlation time for fluc-

[†] Princeton University.
[‡] Bristol-Myers Squibb.

(1) (a) Hutchison, C.; McKay, D. B. *J. Chem. Phys.* **1977**, *66*, 3311. (b) Hurst, G. C.; Henderson, T. A.; Kreilick, R. W. *J. Am. Chem. Soc.* **1985**, *107*, 7294. (c) Yim, M. B.; Makinen, M. W. *J. Magn. Reson.* **1986**, *70*, 89. (d) Mustafi, D.; Makinen, M. *Inorg. Chem.* **1988**, *27*, 3360.
(2) De Beer, R.; De Boer, W.; Van't Hoff, C. A.; Van Ormondt, D. *Acta Crystallogr.* **1973**, *B29*, 1473.
(3) (a) Teleman, O.; Ahlstrom, P. *J. Am. Chem. Soc.* **1986**, *108*, 4333–4341. (b) Chandraskhar, J.; Spellmeyer, D. C.; Jorgensen, W. L. *J. Am. Chem. Soc.* **1984**, *106*, 903–910.
(4) Smith, R. M.; Martell, A. E. *Critical Stability Constants*; Plenum Press: New York, 1976; Vol. 4.
(5) (a) Ducommun, Y.; Newman, K. E.; Merbach, A. E. *Inorg. Chem.* **1979**, *18*, 2754. (b) Martini, G.; Romanelli, M.; Burlamacchi, L. In *Molecular Motions in Liquids*; Lascombe, J., Ed.; Reidel: Dordrecht, 1974; p 371.

0002-7863/92/1514-9600$03.00/0

Table I. ^{1}H Hyperfine Tensors (MHz) and Mn–H Distances (Å) and Hexaquo Mn^{2+}

	a_{iso}	$A^d_{\parallel}$	$A^d_{\perp}$	$A^d_{\perp}$	r (Mn–H)
water, pH 0.07	0.8 ± 0.3	7.4 ± 0.6	−3.7 ± 0.4	−3.7 ± 0.4	2.87 ± 0.1
	0.0	nd[a]	−0.8	−0.8	4.8
MD simulation					2.9, 4.8
$La_2(Mg)_3(NO_3)_{12}\cdot 24H_2O$ (ref 2)	0.87 ± 0.2	7.13 ± 0.39	−3.70 ± 0.22	−3.42 ± 0.17	2.82 ± 0.06
$ZnSiF_6\cdot 6H_2O$ (ref 10)	−0.2 ± 0.2	6.0	−3.1 ± 0.2	−2.9 ± 0.2	3.1
	−0.3 ± 0.2	6.7	−3.8 ± 0.2	−2.9 ± 0.2	3.0

[a] Not determined.

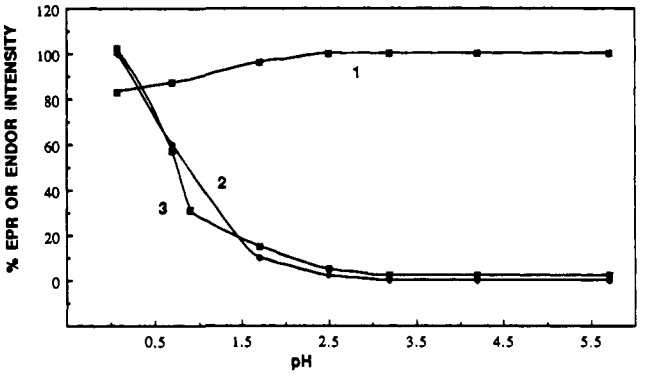

Figure 1. Titration of aqueous $MnCl_2$ with perchloric acid (1) EPR amplitude at room temperature. (2) EPR amplitude of six-line pattern at 100 K. (3) Proton ENDOR amplitude at 10 K.

tuation of the ZFS produced by asymmetrically bound water molecules in the second shell must occur rapidly in the timescale 10^{-11}–10^{-12} s in order to account for the dynamical averaging of the EPR spectrum.[5,6] Although the EPR intensity of Mn^{2+} is sensitive to the asymmetry of the ligand field, it offers no direct means for measuring the solvent structure. The present study provides the first direct structural evidence supporting this model.

When the nuclear and electron magnetic moments are quantized by an external magnetic field, the dipolar hyperfine energy can be given by a simplified expression.[7]

$$h\nu^d = g_e\beta_e g_n\beta_n m_s m_I(3\cos^2\theta - 1)/(r_{12})^3 \qquad (1)$$

(r_{12}) is the average distance of separation and θ is the angle made by the line joining the two magnetic centers (approximated as localized points) and the direction of the external magnetic field. All other terms have their usual meaning. The observed hyperfine splitting must first be separated into the isotropic part (Fermi contact) and the anisotropic part (dipolar).

Results and Discussion

Figure 1 curve 1 shows that the six-line EPR intensity at 300 K of an aqueous $MnCl_2$ solution titrated against perchloric acid is invariant between pH 7 and 2.5; a small 18% decrease occurs betweeen pH 2.5 and 0.07. The decrease may be due to formation of weakly associated ion pairs with the perchlorate anion, as seen with some polyanions such as dithionite.[6]

When the solution is frozen at neutral pH, the six-line EPR pattern disappears and a 600-G broad featureless signal is observed at 0.1% of the solution intensity (not shown). In frozen solutions, as the pH is lowered below 2.5 to 0.07, both the six-line EPR intensity (Figure 1, curve 2) and the proton ENDOR signal (Figure 1, curve 3) grow in parallel. We conclude that the proton ENDOR arises only from the species giving rise to the six-line EPR signal. The pH onset of the modest decrease in EPR intensity of the fluid solution parallels the large increase in EPR and ENDOR intensities of the frozen solutions, suggesting a possible common origin.

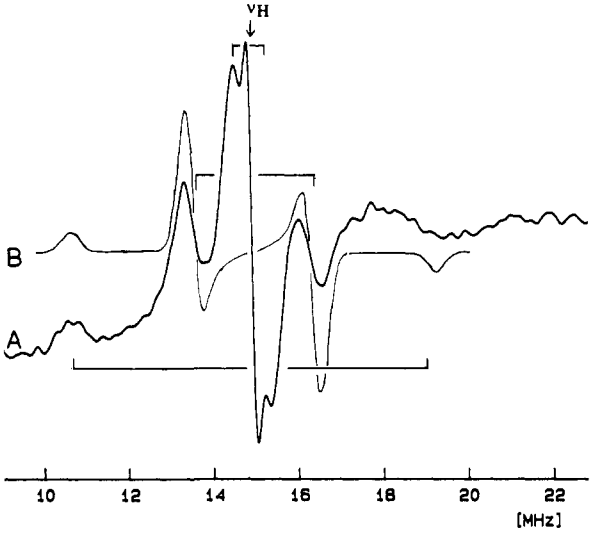

Figure 2. (A) Proton ENDOR of a frozen solution of $MnCl_2$ (0.18 mM) in perchloric acid at pH 0.07. ENDOR conditions same as for Figure 1. The sample is a microcrystalline powder. (B) Computer simulation of the power ^{1}H ENDOR spectrum for $Mn(H_2O)_6^{2+}$ using Mn–H = 2.8 Å, a_{iso} = 0.8 MHz, and a frequency-independent Gaussian line width of 0.2 MHz.

Figure 2A shows the proton ENDOR spectrum for Mn^{2+} in frozen aqueous solution at pH 0.07. There are three resolved pairs of peaks centered at ν_H with hyperfine splittings of 0.8 ± 0.2, 2.9 ± 0.3, and 8.2 ± 0.5 MHz. These were analyzed initially assuming that they arose from a single class of ^{1}H with a rhombic tensor. This failed, as follows. Departure from an axial hyperfine tensor for the symmetrical ^{6}S ground state of $[Mn(H_2O)_6]^{2+}$ in single crystals has been analyzed quantitatively and found to be due to transfer of spin density (ρ) onto the coordinated O atoms.[2] The effect is quite small; the mean nonaxial hyperfine component, defined as $\langle\Delta A^d_{\perp}\rangle/A^d_{\perp} = 0.076$ ($A^d_{\perp} = 3.56 \pm 0.24$ MHz), yields $\rho = 0.0025$ and a correction to the Mn–H distance of only 0.01 Å. In Figure 2, assigning $\langle\Delta A^d_{\perp}\rangle/A^d_{\perp} = 1.1$ (from $A^d_{\perp}$ = 0.8 and 2.9 MHz) yields $\rho > 0.3$ per O atom, and we see that the apparent degree of covalency is grossly out of line with elementary considerations of bonding. These peaks *must* arise from different protons.

The line shapes of the resonance features at 2.9 and 8.2 MHz are consistent with the turning points of an axial hyperfine tensor corresponding to $-A_{\perp}$ and $A_{\parallel}$, respectively.[7] With this choice of assignment, the isotropic hyperfine interaction, obtained from the trace $a_{iso} = (A_{\parallel} + 2A_{\perp})/3$, is 0.8 ± 0.3 MHz, while the dipolar part is 7.4 and −3.7 MHz, as listed in Table I. . Using eq 1 with $|m_s| = {}^1/_2$ and the value of $A^d_{\parallel}$, we calculate the Mn–H distance to be 2.87 ± 0.1 Å. All first-shell protons appear to have the same Mn–H distance within the limits of the method. This implies that the bisector of the HOH angle lies along the Mn–O bond axis.

Confirmation of the spectral deconvolution for the first-shell protons was provided by performing a computer simulation[11] of

(6) Romanelli, M.; Burlamacchi, L. *Mol. Phys.* **1976**, *31*, 115–127.
(7) Carrington, A.; McLachlan, A. D. *Introduction to Magnetic Resonance*; Harper and Row: New York, 1967.
(8) Burlamacchi, L.; Tiezzi, E. *J. Mol. Struct.* **1968**, *2*, 261–270.
(9) Sivaraja, M.; Dismukes, G. C., unpublished results.
(10) Berendsen, H. J. C.; Straatsma, J. P. M.; Van Gunsteren, W. F.; DiNola, A.; Haak, J. R. *J. Chem. Phys.* **1984**, *81*, 3684–3690.
(11) Khangulov, S. V.; Sivaraja, M.; Barynin, V. V.; Dismukes, G. C., unpublished results.

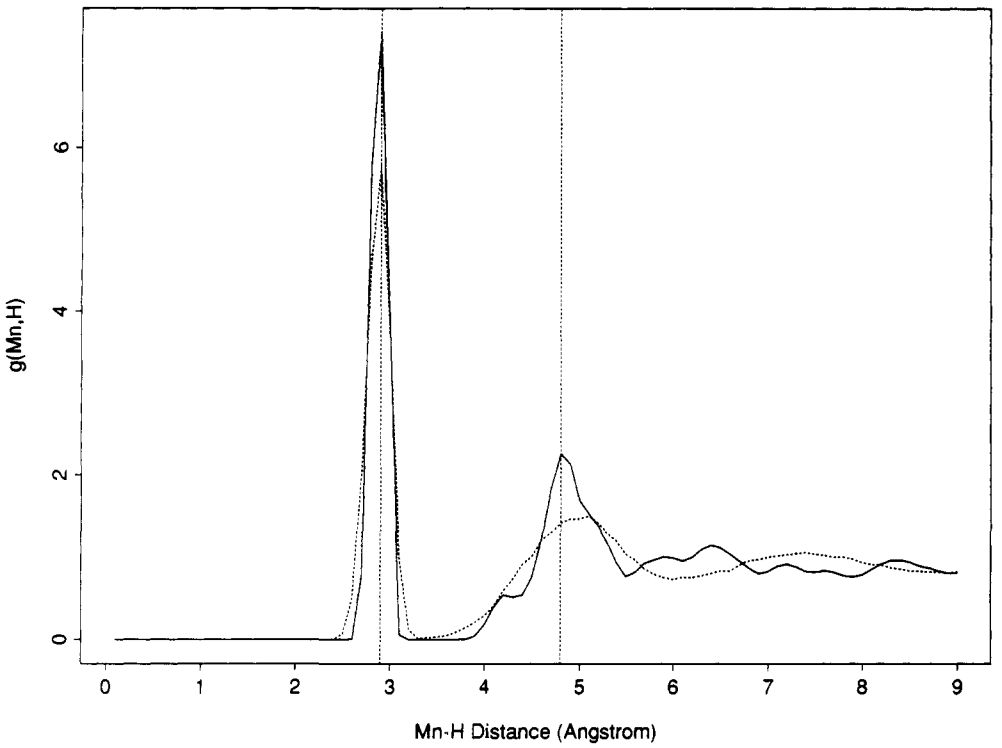

Figure 3. Mn–H radial distribution function of 50 K (solid) and 300 K (dotted) obtained by classical molecular dynamics simulation of Mn^{2+} in a periodic box of 212 water molecules.

the ENDOR spectrum, given in Figure 2B. This included both Fermi contact and point dipolar hyperfine interactions to Mn^{2+}. Powder line shapes where obtained by averaging the angular part of the dipolar interaction over a unit sphere. The parameters used in the simulation given in Figure 2B are Mn–H = 2.8 Å, a_{iso} = 0.8 MHz, and a uniform Gaussian line width of 0.2 MHz. The simulation shown does not include the second-shell protons, nor does it provide for different line widths for the parallel vs perpendicular transitions. The agreement with the positions of the experimental transitions is the basis for the spectral parameter set given in Table I.

Both the isotropic and dipolar hyperfine interactions and the deduced Mn–H distance agree well with the values measured for $[Mn(H_2O)_6]^{2+}$ in the double nitrate crystal lattice[2] $La_2(Mg)_3(NO_3)_{12}\cdot 24H_2O$, as summarized in Table I. In the case of the trigonally distorted crystal lattice of $ZnSiF_6\cdot 6H_2O$, the Mn–H distance increases by 0.13–0.23 Å, while a_{iso} drops to −0.2 to −0.3 MHz. The m_s origin of the EPR transition being pumped in the ENDOR experiment could not be $|m_s| = {}^3/_2$ or ${}^5/_2$, as these yield physically impossible Mn–H distances of 4.12 and 4.88 Å, respectively, for the first-shell protons. Moreover, these should produce eight peaks, not four as is observed.

We considered the smallest splitting of 0.8 MHz as arising either from a second shell of water molecules, or, possibly, from first-shell proton coupling to $|m_s| = {}^3/_2$ or ${}^5/_2$ levels. Taking the second interpretation and using eq 1 with $\theta = 90°$ predicts transitions at 10.9 and 18.2 MHz, respectively; *we reach an inconsistency*. Taking the former assignment with the second-shell protons coupled to the $|m_s| = {}^1/_2$ levels, we obtain with $\theta = 90°$ an Mn–H distance of 4.8 Å. This is physically plausible. A pair of broader lines are also expected for the $\parallel$ tensor component at 1.6 MHz. These should be 5-10-fold weaker and thus would be undetectable, owing to overlap with the intense peak at 2.9 MHz (Figure 2).

In order to judge whether this assignment of the 0.8-MHz coupling is consistent with second-shell water molecules H-bonded to the first-shell molecules, we analyzed the structure of water solvated to Mn^{2+} by a classical molecular dynamics simulation. The simulation used a widely-distributed three-point flexible water model with electrostatic and van der Waals interactions to Mn^{2+} (ref 12). The equilibrium Mn–H radial distribution function is plotted in Figure 3 at 50 and 300 K. At 50 K, the symmetric first shell is comprised of 12 hydrogens at a means distance of 2.9 Å. This distribution is narrow. The structured second shell is comprised of 18 water molecules, peaking at Mn–H = 4.8 Å. The structure becomes dynamically averaged at 300 K as the second shell expands to encompass, on average, 22 H_2O molecules at a mean distance of 5.0 Å. The mean Mn–H distances do not change appreciably below 50 K. These results confirm the assignments given by the hyperfine analysis and also provide coordination numbers.

The agreement is surprisingly good, which may reflect the specific suitability of Mn^{2+} to classical analysis. For example, we have ignored quantum effects in the intermolecular potential which might be important at low temperature for some ions. For Mn^{2+}, however, the bonding is almost exclusively ionic in character, and a simple Coulomb potential seems intuitively plausible. Morever, the symmetrical electronic distribution associated with the ^6S ground state of Mn^{2+} should be realistically described by the spherically symmetric van der Waals and Coulomb potential functions we used. This may not be adequate for other transition-metal ions.

In conclusion, the emergence of highly symmetrical coordination to first- *and* second-shell water ligands surrounding Mn^{2+} in frozen solution appears to be responsible for the simplification and intensification of the EPR signal at low pH, as seen directly by ^1H ENDOR and confirmed by molecular dynamics simulations. These results are also noteworthy because it is unusual to obtain resolved dipolar hyperfine structure in a disordered sample by ENDOR spectroscopy from molecules bound in the second shell.[1c,d] The protons in the second shell are separated by four bonds (2 covalent + 1 H-bond + 1 dative) from the center of spin density.

These results should encourage the application of molecular dynamics simulations to the study of solvation of nonparamagnetic ions for which structural data are less readily available.

Experimental Section

EPR and ENDOR spectra were recorded using BRUKER spectrometers (ESP300 and ER250A). EPR conditions: microwave power, 5

(12) *Discover* biomolecular simulation package V. 260, BIOSYM Technologies, Inc., 10065 Barnes Canyon Road, Suite A, San Diego, CA 92121.

mW, microwave frequency, 9.37 GHz, modulation frequency, 100 KHz, modulation amplitude, 10 G. ENDOR conditions: microwave frequency, 9.44 GHz, microwave power, 5 mW, radio frequency power, 150 W, radio frequency modulation frequency, 12.5 KHz, radio frequency modulation depth, 75 KHz, scan rate, 0.125 MHz/s, number of scans, 30.

Estimates of the packing of water around the Mn^{2+} ion were obtained through classical molecular dynamics simulations of a single Mn^{2+} ion surrounded by 212 water molecules in a 3-dimensional periodic box of 18.621 Å (approximate density of 1.0 g/mL). The simulations were run at constant temperature and constant volume. A three-point flexible water model was used, wherein each atom possessed a partial point charge (O, −0.82 electron units (eu); H, +0.41 eu). The oxygen was a Lennard-Jones 6–12 center (distance of lowest energy interaction for homoatomic approach, $r^* = 3.553$ Å; minimum potential well depth for homoatomic approach, $\epsilon = 0.1554$ kcal/mol), and the hydrogens were a very small Lennard-Jones repulsive center (A^{12} was 1×10^{-8} for the calculation of interatomic repulsion). The geometric means combining rule was used to calculate the interatomic Lennard-Jones interaction parameters. Electrostatic interactions were computed via Coulomb's law utilizing a dielectric of 1.0. The O–H bond stretch and H–O–H angle bend were represented by harmonic potentials with equilibrium values of 0.96 Å and 104.0° and force constants of 540.6 kcal/mol/Å^2 and 50.0 kcal/mol/deg^2, respectively. This water model is available in a widely distributed biomolecular simulation package[12] and has been characterized as being comparable to other flexible water models in its duplication of structural, thermodynamic, and dynamical properties.[13] The manganese ion was represented as a Lennard-Jones 6–12 center ($\sigma = 2.45$ Å, $\epsilon = 0.1212$ kcal/mol) with charge = 2+. The cutoff used for the intermolecular interactions was 10 Å. The simulation was initiated by several hundreds steps of steepest descent minimizations followed by initial assignments of velocities from a Maxwellian distribution at 50 K. A commercially available simulation package was used which employs the leapfrog variant of the Verlet algorithm.[12,14] The system was taken to 300 K in 50 K increments of 1-ps dynamical simulation with coupling to an external temperature bath at the target temperature.[15] For the 50 K run, the temperature was gradually reduced back to 50 K in the same procedure as the heating process. The heating and cooling runs were performed in order to allow for gradual adjustment of the systems to the target temperatures. Once the target temperatures were achieved, the trajectories were allowed to evolve for several hundred picoseconds. The first 30 ps of each simulation was discarded to allow for any further equilibration process.

Acknowledgment. This study was supported by a postdoctoral grant from the American Cyanamid Corporation and research support from the NIH, GM39932.

Registry No. Mn^{2+}, 16397-91-4; water, 7732-18-5.

(13) Alper, H. E.; Stouch, T. R., unpublished results.
(14) Verlet, L. *Phys. Rev.* **1967**, *159*(1), 98.
(15) Berendsen, J. C.; Straatsma, J. P. M.; Van Gunsteren, W. F.; Di Nola, A.; Haak, J. R. *J. Chem. Phys.* **1984**, *81*(8), 3684.

Kinetic EPR Studies of the Decay of *tert*-Butyl Alkoxy, Silyloxy, Germyloxy, and Stannyloxy Nitroxides

Marco Lucarini,[†] Gian Franco Pedulli,*[,†] Angelo Alberti,*[,‡] and Massimo Benaglia[‡]

Contribution from the Dipartimento di Chimica Organica "A. Mangini", Via S. Donato 15, I-40127 Bologna, Italy, and I.Co.C.E.A., CNR, Via della Chimica 8, I-40064 Ozzano Emilia, Italy. *Received March 9, 1992*

Abstract: The kinetics of decomposition of oxynitroxides $Me_3CN(O^•)OMR_3$, with $R_3M = Me_3C$, Bu_3Sn, Ph_3Ge, and Ph_3Si, has been studied by EPR at different temperatures, and the activation parameters have been determined. While the first nitroxide undergoes cleavage at the nitrogen–oxygen bond more readily than at the nitrogen–carbon bond, the organometallic nitroxides essentially fragment with elimination of a *tert*-butyl radical with rates of fragmentation increasing, at ordinary temperatures, along the sequence $Ph_3Ge < Ph_3Si < Ph_3Sn$. A very large reduction of the frequency factor for the decomposition was observed on descending the periodic table. This has been explained in terms of an equilibrium between the nitroxide adduct and its dimer; experimental evidence supporting the existence of this equilibrium has been obtained.

The reduction of tertiary aliphatic nitro compounds to the corresponding alkanes using tributyltin hydride in the presence of radical initiators has been extensively used for synthetic purposes during the last decade.[1-4] Mechanistic studies are consistent with a free radical chain reaction where the key propagation steps are the addition of $Bu_3Sn^•$ radicals to the nitro group and the cleavage of the resulting oxynitroxides, $RN(O^•)OSnBu_3$, into $R^•$ radicals and nitrites.[5,6] As an alternative pathway, it has been proposed that electron transfer takes place between the tin radical and the nitro compound followed by fragmentation of the resulting radical anion.[7-9] This latter mechanism, although not yet universally rejected,[10,11] appears to be unlikely on the basis of a recent report where it was shown by combining oxidation potentials and thermochemical data that the electron-transfer reaction is not a feasible process.[6]

From the synthetic point of view the value of this reaction is a consequence of the fact that the decomposition of the intermediate takes place by cleavage of the carbon–nitrogen (route 1a) bond rather than the nitrogen–oxygen (route 1b) bond.

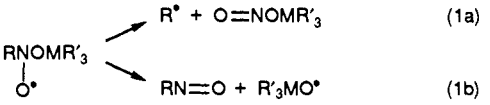

(1a) (1b)

Actually, tris(trimethylsilyl)silane, which is a good substitute for

[†] Dipartimento di Chimica Organica.
[‡] I.Co.C.E.A.

(1) Ono, N.; Miyake, H.; Tamura, R.; Kaji, A. *Tetrahedron Lett.* **1981**, *22*, 705.
(2) Ono, N.; Miyake, H.; Kamimura, A.; Hamamoto, I.; Tamura, R.; Kaji, A. *Tetrahedron* **1985**, *41*, 4013 and references therein.
(3) Ono, N.; Kaji, A. *Synthesis* **1986**, 693.
(4) Neuman, W. P. *Synthesis* **1987**, 665.
(5) Korth, H. G.; Sustman, R.; Dupuis, J.; Giese, B. *Chem. Ber.* **1987**, *120*, 1197.
(6) Tanner, D. D.; Harrison, D. J.; Chen, J.; Kharrat, A.; Wayner, D. D. M.; Griller, D.; McPhee, D. J. *J. Org. Chem.* **1990**, *55*, 3321.
(7) Tanner, D. D.; Blackburn, E. V.; Diaz, G. E. *J. Am. Chem. Soc.* **1991**, *103*, 1557.
(8) Ono, N.; Tamura, R.; Kaji, A. *J. Am. Chem. Soc.* **1983**, *105*, 4017.
(9) Dupuis, J.; Giese, B.; Hartnung, J.; Leising, M. *J. Am. Chem. Soc.* **1985**, *107*, 4332.
(10) Russell, G. A. *Adv. Phys. Org. Chem.* **1987**, *23*, 303.

0002-7863/92/1514-9603$03.00/0